Influence of poly(styrene sodium sulfonate) grafted silicone breast implant's surface on the biological response and its mechanical properties

M. Lam, Romain Vayron, Rémi Delille, V. Migonney, C. Falentin-Daudré

Version of Record: https://www.sciencedirect.com/science/article/pii/S235249282200191X
Manuscript_ce575759e7fd62ac0ba0e5f2f3c66137

Influence of poly(styrene sodium sulfonate) grafted silicone breast implant's surface on the biological response and its mechanical properties

M. Lam[1], R. Vayron[2], R. Delille[2], V. Migonney[1], C. Falentin-Daudré[1]*

1 LBPS/CSPBAT, UMR CNRS 7244, Institut Galilée, Université Sorbonne Paris Nord, 99 avenue JB Clément 93430- Villetaneuse, France.
2 LAMIH, UMR CNRS 8201, Université Polytechnique Hauts-de-France, Valenciennes, France.
*Corresponding author : falentin-daudre@univ-paris13.fr

ABSTRACT

Prior to its commercialization, a biomaterial must fulfill the regulation in place. The International Organization for Standardization outlines the requirements needed for a material in order to guarantee safety and quality. In previous work, we have successfully grafted a bioactive polymer known as poly(styrene sodium sulfonate) – (polyNaSS) on silicone breast implants' surfaces using UV irradiation.

This paper intends to study the effect of the polyNaSS grafting parameters. It includes the study of (i) the effect of only UV irradiation and (ii) the presence of the polyNaSS grafted silicone on both the mechanical properties of the material and the biological response using the L929 fibroblast cell line for biocompatibility investigations. PolyNaSS aims to overcome the lack of biocompatibility issues, but the grafting process should have a minimal impact on the surface's properties.

The tensile strength and swelling tests showed no apparent modification before and after grafting in crosslinking densities and elasticity moduli. That confirms the impactless aspect of the grafting protocol on the material's mechanical properties. Surface roughness was investigated by atomic force microscopy to understand cell behavior on surfaces upon various treatments. Biocompatibility tests showed that the grafting of polyNaSS significantly enhanced cell adhesion and viability compared to a non grafted silicone. Overall, polyNaSS confers a highly suitable surface for fibroblasts, demonstrating their active forms (spindle-shaped). This

was assessed by optical microscopy, scanning electron microscopy, and atomic force microscopy.

KEYWORDS: silicone, implant, mechanical properties, cytotoxicity, cell proliferation

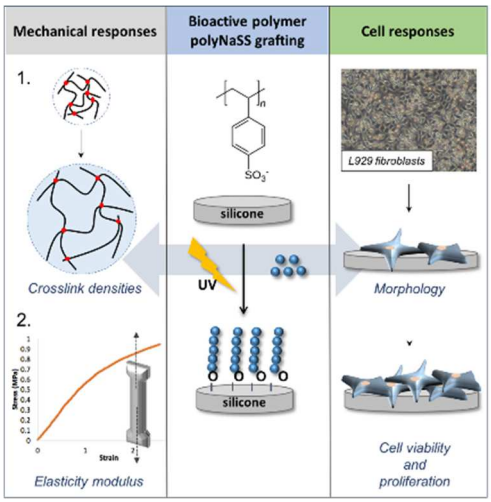

Table of contents

INTRODUCTION

Biomaterials consist of a wide range of materials used in the biomedical field to supply, support, or replace dysfunctional organs or tissues [1]. With a synthetic or natural origin, the contact of such objects with the biological medium may lead to adverse reactions from the organism resulting in more or less severe pathologies [2]. For example, silicone materials, also referred

as poly(dimethylsiloxane), are among the most widespread polymeric materials in the medical field [3][4][5] and mainly for breast implants [6][7]. However, silicone materials are not entirely safe despite all the precautions taken and may cause severe damages to patients.

Due to its physicochemical features, silicone suffers from a lack of biocompatibility resulting in poor bio integration in the body. In addition, the inherent hydrophobicity of the material promotes the adsorption of non-specific proteins [8]. At first, a physiological capsule is formed around the implant as a natural healing procedure to isolate it from the system. Still, the capsule can evolve to a more critical and pathological grade called the capsular contracture (CC), which is associated with bacterial infection [9]. Its severity is evaluated with the Baker classification (I-IV) that relies on the capsules' hardness, painful degree, and skin deformation [10]. Studies have shown that advanced stages of CC are correlated to the implant's roughness and are often encountered with smooth implants rather than with macro-textured implants [11]. Lately, emerging cases of a T-cell non-Hodgkin lymphoma, known as Breast implants associated with large cell lymphoma (BIA-ALCL) [12], appearing exclusively on textured prostheses, have led to reconsider the safety of this type of implants [13][14]. The first case of BIA-ALCL was identified in 1997 [15], and today, nearly 1000 cases have been reported worldwide [16]. According to the U.S Food and Drug Administration (FDA), the risk of BIA-ALCL was estimated between 1/2832 and 1/30000, and was shown to increase for textured implants [16]. The lymphoma is described by a more rigid and tightened capsule around the implant, the swelling, and accumulation of fluid nearby, change in size and shape, and inflammation of the surrounding tissues. The origin of these complications remains unclear, but hypotheses have been suggested to decipher it, including the immune response, genetic predisposition, hematoma, inflammation, and bacterial infections [17–20]. Overall, these complications most likely stem from poor integration of the implant.

To this day, numerous strategies have been developed to improve the biocompatibility of silicone material with coatings or covalent surface modifications by either grafting "from" or grafting "to" methods [21].

In this context, the LBPS team has recently developed a simple way to modify silicone surfaces by grafting a bioactive polymer, the polystyrene sulfonate sodium (polyNaSS). This polymer is known for its wide biocompatibility and its antibacterial action. The grafting strategy relies on a grafting "from" approach onto smooth silicone breast implants shell under UV irradiations [22]. Qualitative and quantitative methods have highlighted the covalent grafting (Attenuated Total Reflectance Transform Infrared Spectroscopy/ATR-FTIR, scanning electron microscopy/SEM, X-ray photoelectron spectroscopy/XPS, colorimetric assay, contact angle measurements). The mechanism involves an **activation step** where hydroxyls (-OH) reactive groups are created under UV, followed by a **radical polymerization step** of the NaSS monomers still under UV (Figure 1). Thanks to its sulfonate (SO_3^-) groups, the polyNaSS has proved its efficiency by improving biocompatibility in *in vitro* and *in vivo* studies on different surfaces, *e.g.,* titanium and its alloys or polymers-based surfaces [23–25].

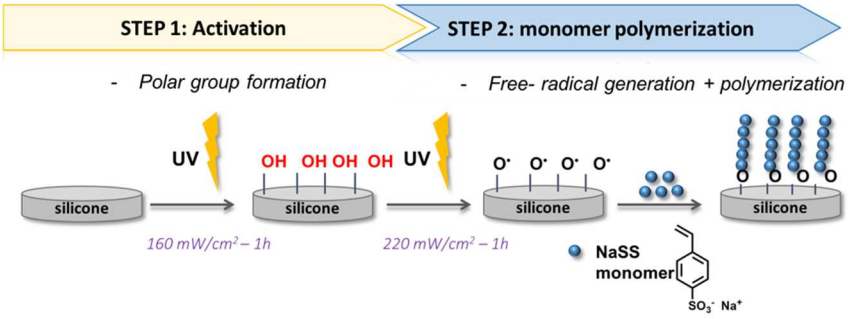

Figure 1: Mechanism of polyNaSS grafting on silicone surface

Silicone materials are highly resistant elastomers, *i.e.,* soft-rigid materials possessing excellent mechanical properties due to their flexibility controlled by the crosslinking density [26]. However, specific requirements need to be fulfilled by biomaterials before any marketing authorization. From this perspective, verifying each parameter involved in the polyNaSS

grafting protocol is essential to ensure that the whole functionalization process does not significantly alter the material's mechanical properties. Moreover, the grafting protocol involves using UV irradiation known to increase material ageing [27] and mechanical weakness leading to implant failures/ruptures or gel leakage [28].

The following study investigates:

1) The influence of the grafting parameters (UV irradiation, presence of polymer) on silicone initial **mechanical properties**.

2) The influence of the grafting parameters (UV irradiation, presence of polymer) on the **biological response**.

Throughout this work, three conditions have been studied and compared for each experiment: Non-grafted, UV-control, and polyNaSS grafted.

MATERIAL & METHODS

- Non-grafted silicone samples preparation

Silicone materials were extracted from medical-grade smooth breast silicone implant shells (Figure 2). After cutting into 3 x 1 cm^2 surfaces, the samples were washed in distilled water (dH_2O) several times for 24h to remove residual dust and eventual impurities. Subsequently, samples were then dried in a 37°C oven for two hours. Then for the experiments, 1 cm diameter silicone disks were cut.

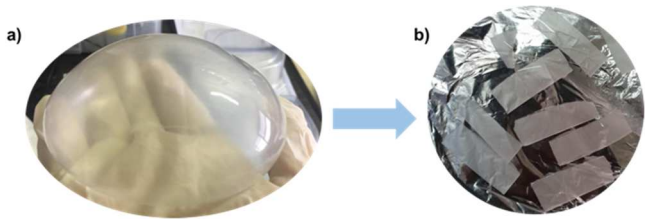

Figure 2: Material used - (a) empty silicone breast implant shell (b) washed silicone samples

- UV-Grafting of polyNaSS on silicone surfaces

First step - ACTIVATION: in an argon-degassed distilled water, silicone disks (Ø1 cm) were irradiated under UV at a power of 160 mW/cm^2 for 1 hour using a low-pressure-mercury lamp – 365nm (Lot Oriel) [22].

Second step - POLYMERIZATION: UV-activated samples were then transferred into an argon-degassed aqueous NaSS monomer solution ([NaSS]=0.35M) and exposed again to UV irradiation at a power of 220 mW/cm^2 for one hour under stirring [22]. The resulting polyNaSS grafted surfaces were cleaned thoroughly in dH_2O for 24h to remove the excess of polyNaSS. Samples were then dried and stored in a 37°C oven. The monomer, Sodium styrene sulfonate was purchased from Sigma-Aldrich.

- UV-control silicone samples preparation

Cleaned silicone samples have undergone two successive UV irradiation for 2 hours without monomers (activation – 1h at 160 mW/cm^2 + polymerization – 1h at 220 mW/cm^2).

- Mechanical tests

Tensile strength test : Five specimens (H3-type) were made using a punch for each condition (Non-grafted, UV-control, and UV-Grafting of polyNaSS samples). Experimental tensile tests were conducted at room temperature to obtain the stress-strain response of each sample. The sample can only be maintained by its extremities. That avoids applying initial strain and stress to the gel sample.

The different tensile tests were solely conducted on an ElectroPuls E3000 electro-magnetic machine. This machine possesses a linear stroke of 60 mm and a dynamic load capacity of 3 kN. However, the material nature requires to use a mono-axial load cell with a calibrated measurement of 250 N with an error of +/- 0.1N. Due to the large strain of the material and limit stroke, the gauge section is 17 x 4 mm with a thickness of 0.5 mm.

Tensile tests were performed with a velocity equal to 4 x 10^{-3} s^{-1} equivalent strain rate. A particular device is set on the machine to ensure a constant displacement rate during sample deformation. Digital Image Correlation is employed using a camera (Manta G: 12.4 Million pixels, full resolution: 4112 x 3008). Pixel size for testing is 0.0245mm. White and black spots painted along the sample length contribute to the direct measurement of transverse and longitudinal strain in the function of time in the gauge area. The camera frame rate was synchronized with the force data acquisition rate. All these measuring tools enable us to evaluate the accurate stress-strain material response with high accuracy.

Swelling procedure : Swelling experiments were performed using Tetrahydrofuran – THF (Thermo Fischer) as the swelling solvent. 2 x 1 cm^2 sized silicone samples were completely immersed into an excess volume of THF at room temperature. Then, samples were taken out every 30 seconds, and their dimensions were quickly measured to minimize solvent evaporation rate. The experiments were ended when a plateau was reached, indicating a nil size variation. The maximum swelling rate was then obtained. The swelling study was performed at least in triplicate in the same experimental conditions.

Equation 1: Swelling rate formula

$$Swelling\ rate = \frac{L}{L_0} * 100$$

L_0: initial length
L: length in time (t)

Equation 2: Flory-Rehner equation

$$C_d = \frac{1}{M_c} = \frac{-[ln\ ln\ (1 - v_2)\ + v_2 + X_1 v_2^2}{V_1 \rho (v_2^{\frac{1}{3}} - \frac{v_2}{2})}$$

C_d: crosslink density ($mol.g^{-1}$)
M_c: molar mass between two crosslinks ($g.mol^{-1}$)
X_1: Flory-Huggin interaction parameter
V_1: solvent molar volume
v_2: fraction of swollen polymer
ρ: density

- Surface characterizations

Scanning electron microscopy (SEM): Cell morphology and spreading were assessed using a HITACHI TM3000 SEM. The observation of cell shapes and distribution on studied silicone surfaces were characterized by imaging several areas on the same sample after fixation using 4% formaldehyde in phosphate-buffered saline (PBS, Gibco)

Atomic force microscopy (AFM): Surface topography and roughness were evaluated using the Brüker Multimode 8 AFM coupled with the Nanoscope V controller (Brüker). Images were taken in the Scan Assyst mode in air, with a silicon nitride probe scanasyst-air (spring constant of 0.40 N/m; Resonant frequency of 70 kHz). The scan size was set to 10 µm x 10 µm with a scan rate of 0.997 Hz. The image resolution was set to 1024 x 1024 pixels. Image treatments and roughness parameters were determined with Gwyddion® software.

- Biological assays

In this paper, all the cell culture experiments were done using the standard Mouse fibroblast cell line L929. The cells were incubated in Dulbecco's Modified Eagle Medium – DMEM (Gibco) at 37°C in humidified air containing 5% CO_2.

- Sample's preparation

Before experiments, samples should undergo a conditioning step to achieve physiological pH equal to 7.4. Samples were successively washed in a 1.5M sodium chloride (NaCl) solution, 0.15M NaCl solution, and a PBS solution. The samples were washed three times for 3 hours each in each solution. Then, the surfaces were rinsed with pure water for 10 minutes. Finally, the samples were air-dried and sterilized under UV radiation (30 W): each side of the sample was exposed for 15 minutes.

- Cell medium preparation

It is important to ensure an ionic and protein equilibrium at the silicone's surface before cell seeding. Therefore, samples were first left in a non-completed medium of DMEM for 6h at 37°C and 5% of CO_2, then kept overnight in a complete medium of DMEM and 10% of Fetal Bovine Serum (FBS, Gibco) in the same conditions.

For all the biological assays, cell-cultured on tissue culture polystyrene (TCP) wells were used as references and are referred as "controls" in the text.

MTT assay: Cells Mitochondrial activity is used as an indicator of cell viability. The mitochondrial dehydrogenases reduce the yellow tetrazolium salt(3-(4,5-dimethylthiazol-2-yl)-2,5-diphenyltetrazolium bromide) (MTT, Sigma) to purple formazan crystals. Silicone samples and cells were incubated for 24h at 37°C in a 24-well TCPS with a density of 5 x 10^4 cells/mL. MTT solution is prepared by dissolving a pre-calculated amount of MTT powder in a corresponding volume of DMEM without phenol red indicator. Then, 100 µL of the prepared MTT solution (5 mg/mL) was added to each well completed with 400 µL of DMEM and incubated for 4 h at 37°C. Cell media was then discarded, and wells were rinsed with 400 µL of PBS. 350 µL of dimethyl sulfoxide (DMSO) was added to decomplex the formazan crystals on the surfaces, and absorbance was measured at 570 nm using a microplate reader (ELx800, BioTek). The viability rate (VR) was calculated using the following relation:

$$VR = \frac{(OD_s - OD_b)}{(OD_c - OD_b)} * 100$$

OD_s stand for the light absorbance of the samples, OD_c is the light absorbance of the positive control, and OD_b is the light absorbance of the negative control. Three samples were used per condition, and the statistical significance was established by one-way ANOVA (p=0.01).

Morphology assays: Fibroblasts' shapes and spreading onto silicone were studied on day 1, day 3, and day 7 (for each condition n=3 at each time point). Samples and cells were incubated in DMEM media. At the different times, samples are taken out to observe the cell's spread under standard optical microscopy (Nikon Eclipse 80i microscope). For SEM imaging, the media was removed from each well, and the surface was rinsed with PBS. Next, cells were fixed on the sample's surface with formaldehyde (Sigma-Aldrich) for 30 minutes, rinsed with Milli-Q ultrapure water for 5 minutes, and stored at 4°C before surface analysis (SEM, AFM).

Statistical *analysis:* All experiments were performed with 3-6 samples each time. Statistical difference was estimated with p-value or Anova analysis for mechanical data.

RESULTS and DISCUSSION

1. Mechanical response

1.1. Tensile strength tests

Silicone polymeric materials are flexible, highly resistant to stress deformation, and exhibit low elasticity modulus. Nevertheless, their mechanical properties can be deeply impacted by UV exposure, *e.g.,* ageing and hardening through increased crosslinking degree [27][29]. In this study, the grafting of polyNaSS aims to improve the implant's bio-integration inside the body [25]. However, the grafting technique mainly involves UV light with irradiances varying between 160 and 220 mW/cm^2. Verifying the conservation of the initial material properties appears necessary to ensure "still-in-the-norm" breast implants. Tests were carried out according to the ISO 37:2017 or ASTM D412-16 standards [30]. The stress-strain deformation curves obtained are shown in Figure 3, and the numeric data are summarized in Table 1. The slope of the curve's first part gives the value of the Young modulus. The obtained values for the different groups are very close and vary around 1.9MPa. Anova-test analysis showed no significant difference (F-value = 0.26), leading to the belief that UV has no significant effect on silicone elasticity modulus.

Table 1: Elasticity moduli values of the different groups of silicone

	Non-grafted	UV-control	polyNaSS grafted
Young modulus (MPa)	1.89 ± 0.19	1.97 ± 0.10	1.93 ± 0.11

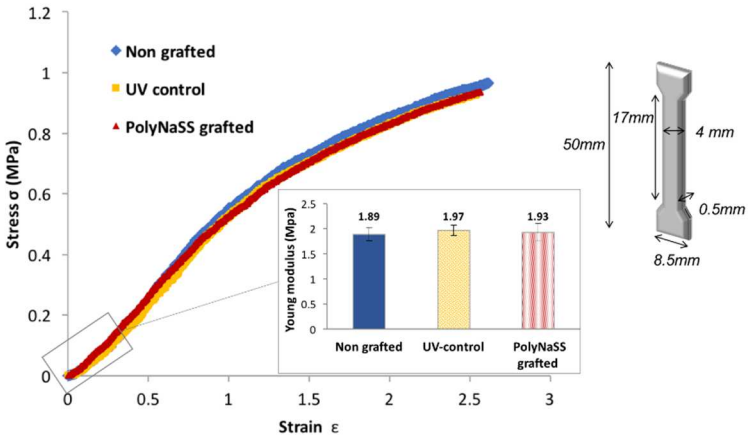

Figure 3: Stress=f(strain) curve of different groups of silicone samples

1.2.Swelling tests

A polymer swelling test was carried out to comfort the previously observed results and highlight the mechanical properties of the material's 3D network. The technique relies on the principle where solvent molecules interpenetrate the polymer chains resulting in swelling. As an elastomer, silicone can undergo swelling in various organic solvents with solubility parameters between 7.3-9.5 $cal^{1/2}.cm^{-3/2}$, such as tetrahydrofuran, toluene, chloroform, or cyclohexane, for example [31]. The higher the swelling rate is, the less the silicone is crosslinked. In this publication, we evaluate the impact of UV irradiation on the material's crosslinking degree through the variation of swelling rate using tetrahydrofuran. The crosslinking density is determined when the swelling reaches an equilibrium (plateau). The maximum swelling degree of the network is related to the crosslinking degree. These experiments were carried out the same day to minimize errors due to experimental conditions (temperature, pressure, humidity).

The swelling rate as a function of time is illustrated in Figure 4. In the first minutes (0-2min), we observed a rapid swell. Then, the swelling slowed down (2-10min) until it stabilized and reached an equilibrium state. At this point, no more solvent molecules could penetrate the 3D network.

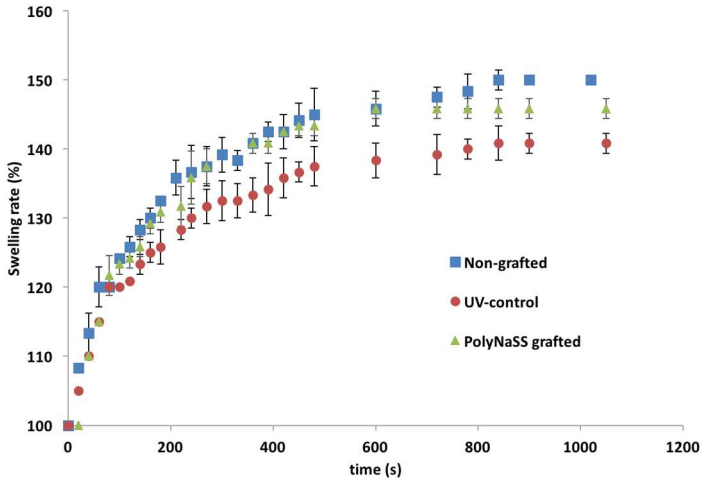

Figure 4:Volume swelling=f(t) curves of the different silicone groups

Comparing this swelling test for the three different conditions revealed a slight variation between the different groups. Compared to the non-grafted condition, a slight decrease of the maximum value is observed with UV-control and polyNaSS grafted silicone with, respectively, a max swelling rate of 150%, 139%, and 140%. The relative difference between non-grafted and UV-control was 8.5%, and between non-grafted and polyNaSS grafted, it was evaluated to 4.5%, which is considered relatively low. Therefore, UV-control is considered quite an "extreme" condition, which was not the most accurate regarding the final application, but is essential to understanding and explaining other results.

Regarding this, the difference between non grafted and polyNaSS grafted groups appears not significant. These results support the previous observations where elasticity moduli were very close in those different conditions. The inverse of the swelling rate also provides the crosslinking density varying around 2-5 x 10^{-4} mol.g^{-1} with obviously a higher value for UV-

control group (Table 2). Furthermore, the polymer chains' average molar mass between two crosslinkers could be determined with the Flory-Rehner equation [32]. The calculated crosslinking densities and the average molar mass ($g.mol^{-1}$) of each condition are slightly different in the range of 2000-4000 $g.mol^{-1}$ (Table 2). These results agree with the values found in the literature [33].

Table 2: Crosslink densities and average molar mass of polymer network of different silicone groups

	Non-grafted	UV-control	polyNaSS grafted
Crosslink density ($mol.g^{-1}$)	2.67×10^{-4}	4.84×10^{-4}	3.45×10^{-4}
Molar mass Mc ($g.mol^{-1}$)	3752 ± 37.14	2066 ± 20.45	2900 ± 28.70

In brief, from a mechanical point of view, the grafting of the bioactive polymer can be safely performed without damaging and altering the silicone shell initial properties.

2. Surface topography and roughness

Breast implant shells studied in this paper are commercialized as smooth implants. Macroscopically, the outer surface is smooth and brilliant, whereas the inner side displays a rougher aspect making the surface opaque. In the same way, scanning electron microscopy images have shown no visible roughness at the microscopic scale [26].

However, more in-depth analysis using atomic force microscopy (AFM) revealed another surface aspect: the non-grafted silicone surface appears rough at the nanoscale, as presented in figure 5a. Indeed, qualitatively, the color contrasts observed on the 2D image revealed a relative variation of highs. 3D representation clearly showed that the surface was made of a succession of sub-micrometric peaks and valleys with a roughness of 14.4 ± 1.1 nm (Figure 5d).

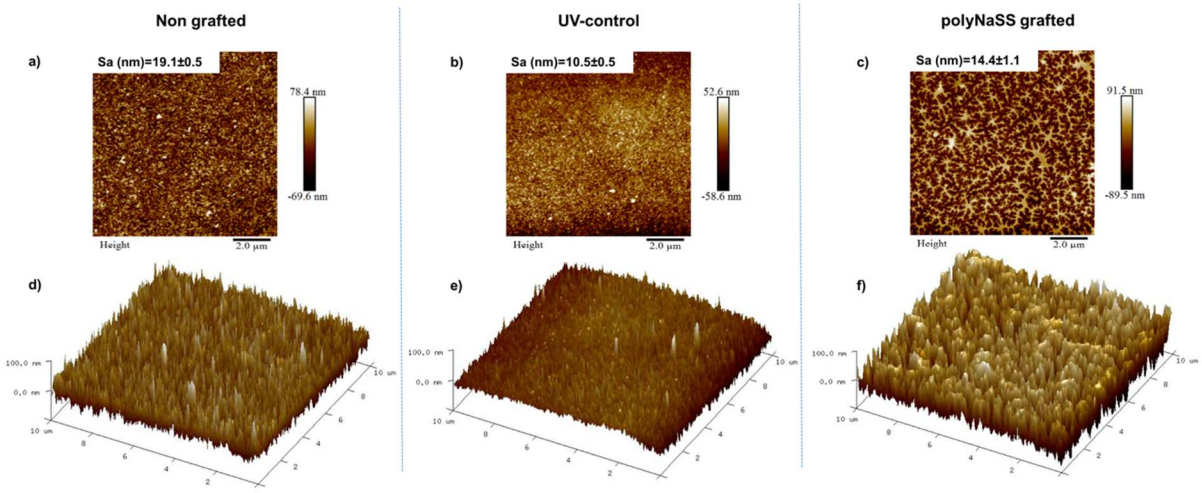

Figure 5: AFM 2D (a,b,c) & 3D images (d,e,f) of silicone surface topography

The roughness parameter Sa is used to evaluate the global surface roughness defined as the arithmetical mean high. Compared to a non grafted surface, UV irradiations smooth the surface with a decrease of Sa from 19.1 ± 0.5 nm to 10.5 ± 0.5 nm. Interestingly, a polyNaSS grafted surface displays another surface tendency. The surface is made of significantly thicker peaks and valleys (3D), as shown in Figure 5f. On the corresponding 2D representation, polymer chains are present at the top of the peaks and connect with another chain forming a network. These observations are essential to explain later cell adhesion results. The literature has genuinely demonstrated that a rough surface enables better cell attachment thanks to cavities' presence [34]. On the other hand, this could also favor bacterial adhesions [35][36].

3. Cell response

Cell culture experiments have been performed using the standard mouse cell line L929 fibroblasts to evaluate silicone surfaces' biocompatibility.

3.1.Cell viability

Cell viability is part of the cytotoxicity test required to evaluate biomaterial devices. ISO 10993-5: 2009 standards state to 70% the limit above which a material is qualified as non-cytotoxic

[37]. Silicone-based materials are commonly known and used for their wide acceptable biocompatibility [7].

The MTT assay measures cellular metabolic activity to indicate cell viability and cytotoxicity. It highlights the number of cells still alive once in contact with the surfaces. Cell viability percentage was calculated with the optical density measured (OD) reported to the silicone disk area.

The results showed an apparent increase of cell viability when in contact with polyNaSS grafted surfaces (Figure 6). This is an expected result as it has already been demonstrated on titanium surfaces [25]. Comparatively to non-grafted surfaces, the grafting of polyNaSS has increased the viability from 79.7% to 110.8%. The high viability rate of bare surfaces demonstrated once again the acceptable biocompatibility of medical-grade silicone materials.

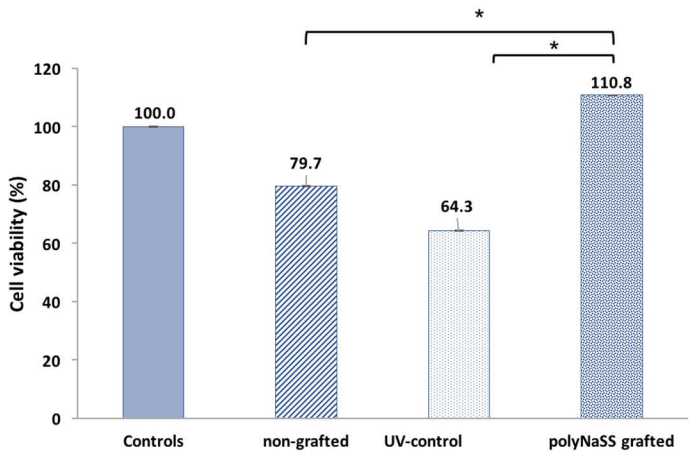

*Figure 6: Viability rates of fibroblasts on different silicone surfaces (*p-value < 0.05%)*

Interestingly, UV-control surfaces exhibited the lowest viability rate (64.3%). This lower rate could be clarified and explained by the observations made on the previous AFM image. As UV tends to re-smooth or flatten silicone surfaces (Figure 6), cell viability on a UV-treated surface decreased because cell adhesion is more favored when the surface is rough.

To sum up, these outcomes showed that no matter the treatment conditions, viability rates are well above the 70% limit for cytotoxicity as recommended by ISO 10993-5: 2009 (Biological evaluation of medical devices) with distinctly greater viability with the presence of the bioactive polymer. These observations match Li *et al*. results where silicone surfaces have enhanced fibroblast viability [38].

3.2.Cell morphology

Fibroblasts' shape, spreading, and morphology consist of interesting indicators regarding surface suitability. Initially, fibroblasts are round-shaped. However, their evolution to an elongated shape reveals a more favorable surface where the cells are free to develop and proliferate [39]. Inversely, cells tend to keep their spherical shapes when the surface is not affine.

- **Cells' morphology under optical and scanning electron microscopies**

The experiments observed the fibroblasts' morphology and density on day 1, day 3, and day 7 of incubation (Figure 7). Imaging under optical microscopy allows better visualization and appreciation of fibroblasts' shapes with the color scale and contrast definition. SEM imaging enables the appreciation of the homogeneity of the cell coverage on the total surface.

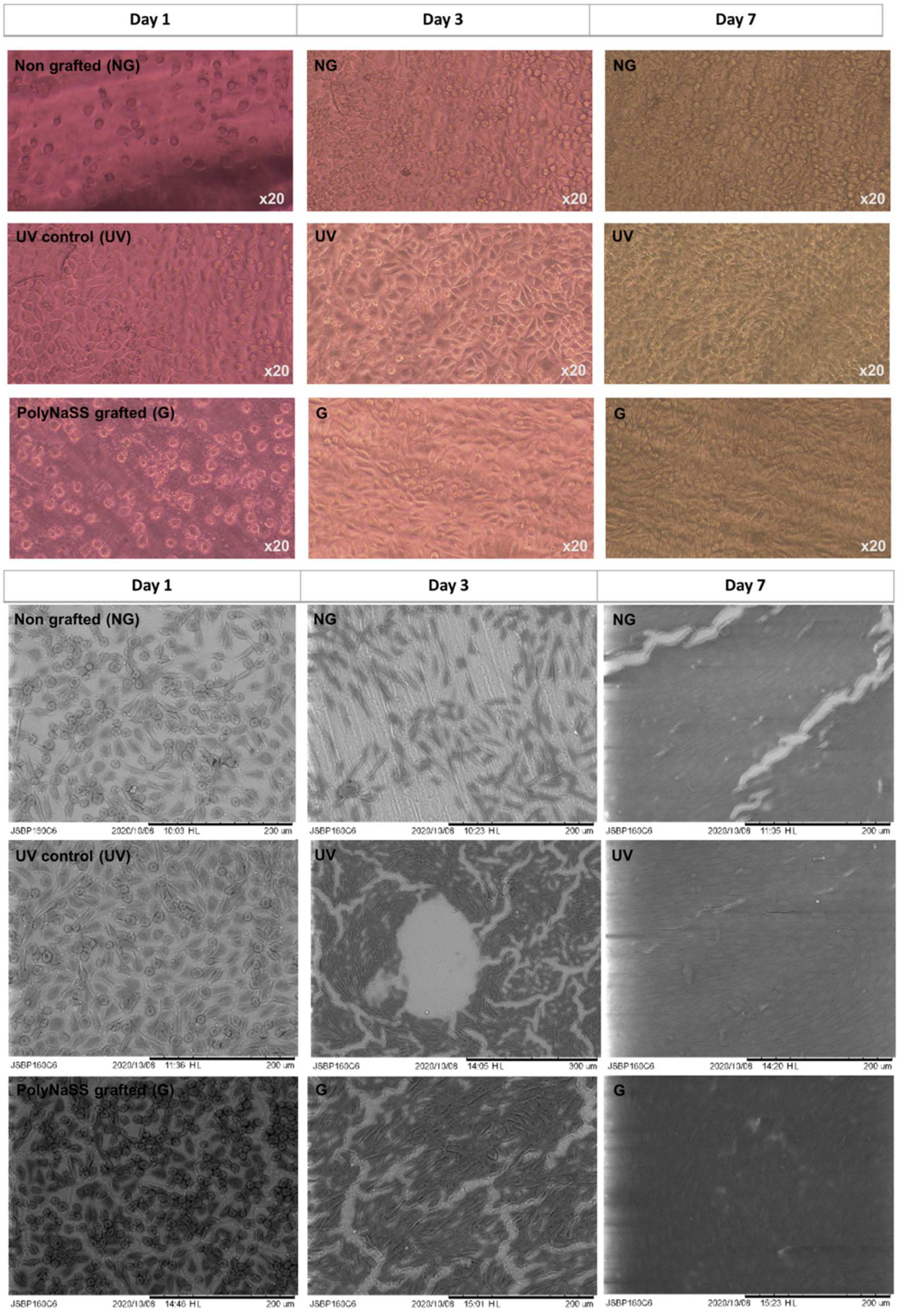

Figure 7: Optical & scanning electron microscopies images of fibroblasts' morphology on different silicone substrates at different time points

On day 1, for the three conditions, well-delimited round-shaped fibroblasts were observed. Over time, progressive elongation of cells' shape was observed and more intensely visible on UV-control and polyNaSS grafted samples (Day 3). After a week of incubation, a more significant morphology change was observed on polyNaSS grafted silicone. Most cells are spindle-shaped, large, and flattened all over the surface. Contrarily, at the same time point on bare silicone, cells are more numerous but still round-shaped. These differences may be attributed to the biocompatible property of polyNaSS that enhances cell development compared to non-grafted silicone surfaces. Interestingly, UV-control surfaces behave as an intermediary as both round and elongated cells were seen. To that extent, we prove that polyNaSS enhances cell adhesion and is more likely to promote cell ingrowth later on.

Over time, added to cell morphology changes, an increase in cell density was also qualitatively notable. On day 3, cells were more numerous because they had more time to settle onto the surfaces than on day 1. Interestingly, a difference was notable: on polyNaSS grafted silicone, the cell density was higher than the other two and began to gather into "grapes."

Finally, on day 7, the surfaces were fully covered by cells, and very few open spaces on grafted surfaces were observable. In contrast, on non-grafted and UV-control surfaces, we can still observe empty areas with no visible cells: the coverage here is less homogeneous.

- **A closer look at a single cell using atomic force microscopy (AFM)**

Atomic force microscopy is a precise and high-resolution technique that gives more detailed information about the adhered cells' size and their nearby interactions at different time points.

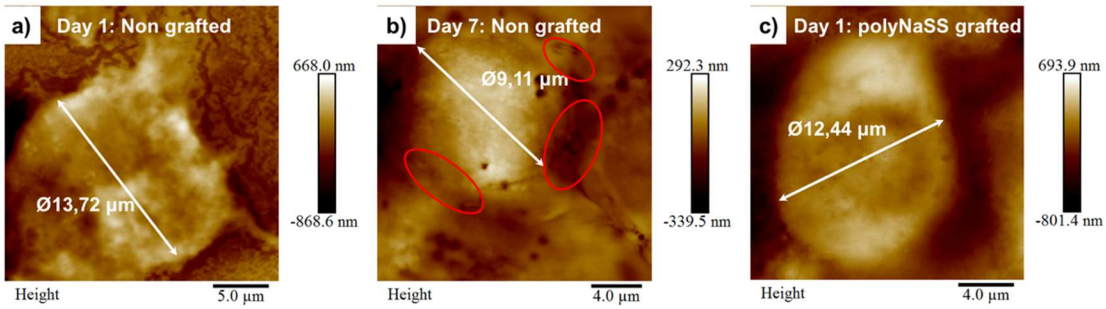

Figure 8: AFM captures of a single fibroblast (a) on a non-grafted surface - day 1, (b) on a non-grafted surface with closely surrounding cells (red circles) - day 7, (c) on a polyNaSS grafted surface – day 1

The difference in a non-grafted on day 1 and day 7 relies on the cell density higher after a long incubation period. As cell densities increased, they retracted in size (9.1 µm versus 13.72 µm on day 1). Along with that, as seen in figure 8 b), neighboring cells have their membranes very closed (red circles). Finally, due to the high cell density, it was impossible to capture a clear image of cells on day 7 on grafted samples.

In figure 9 are represented AFM captures of adhered cells on polyNaSS grafted surface. For the same reason as above, for clearer and high resolute captures, cell morphologies have been taken on day 3. This closer look confirms the observation made with SEM images when we have pointed out elongated fibroblasts in contact with polyNaSS grafted surface. On day 3, cells began spreading well, and spindle-shaped forms were observed. Figure 9a-c showed the various spreading shapes of fibroblasts when in contact with a suitable surface going from spindle to a more elongated shape with extended dimensions than non-grafted conditions.

Another interesting observation is made by zooming in figure 9a (Figure 9a-i). It reveals a kind of interconnection between two cells wall in the form of fibers. This observation is particularly marked in Figure 9d, where the bonding area seems to be more intense. Finally, figure 9e showed deeper interaction as if two distinct cells start to reunite. Overall height AFM imaging enables us to appreciate more in detail the way cells spread on an ideal surface and their interaction with their neighbor.

Furthermore, peak force captures (Figure 9e-f) highlighted the presence of lamellipodia at the cell's extremity. Also, fibers covering the cell surface are observed, and they can be attributed to actin fibers responsible for cell movements.

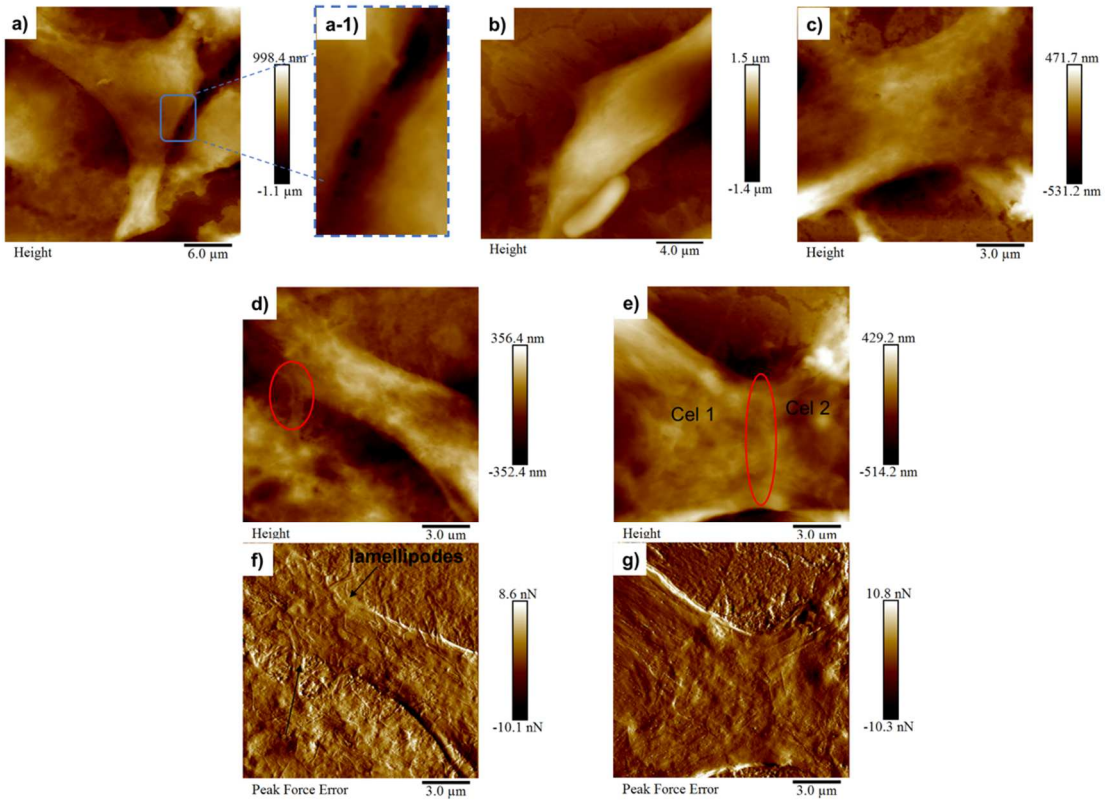

Figure 9: AFM heights images (a-c) of fibroblasts' various shapes on polyNaSS grafted silicone surfaces. AFM heights images (d-e) on fibroblasts' extremities in connection with another fibroblast with the corresponding peak force error captures (f-g).

All-inclusive, these exciting results underline et enforce the fact that cell adhesion and behavior are closely related to surface composition. First, MTT quantitatively confirms better cell viability when the surface is grafted with the bioactive polymer. Second, through various microscopy techniques, it was supported that polyNaSS grafted surface promotes cell spreading.

These cytotoxicity and biocompatibility assays firmly enforce sulfonate groups' presence in improving cell development. Grafted polyNaSS consists of an appropriate environment for fibroblast development to freely spread and grow. In addition, it has enhanced cell viability

compared to a bare silicone surface. These results are encouraging and should be deeply completed with bacterial assays.

CONCLUSION

This article aims to study the impact of UV-induced polyNaSS grafting on (1) the mechanical properties of silicone and (2) the biological response by comparing the results with non-grafted surfaces taken as reference.

It has been successfully shown that the grafting of polyNaSS on silicone surfaces has significantly improved its biocompatibility without seriously damaging the surface by altering its mechanical properties. The bioactive polymer has greatly enhanced fibroblast cell viability and has conferred a suitable surface for cell adhesion and spreading. From a mechanical perspective, despite the intensive use of UV irradiations in the grafting process, the material has conserved its initial properties. By grafting the polyNaSS, the surface was not significantly altered, which is an excellent point to be highlighted.

Finally, the present results are promising and encouraging. *In vitro* bacterial assays and many other studies are under investigation as PolyNaSS specificity also relies on its antibacterial property.

Acknowledgments: This research was supported by the French Ministry of National Education, Higher Education and Research. Thanks also to the University of Sorbonne Paris Nord.

REFERENCES

[1] B.D. Ratner, A. Hoffman, F. Schoen, J. Lemons, Biomaterials Science: An Introduction to Materials in Medicine, 2nd ed., Elsevier Academic Press, 2004.

[2] D.J. Stickler, R.J.C. McLean, Biomaterials Associated Infections: The Scale of the Problem, (n.d.) 17.

[3] A. Gokaltun, M.L. Yarmush, A. Asatekin, O.B. Usta, Recent advances in nonbiofouling PDMS surface modification strategies applicable to microfluidic technology, Technology. 05 (2017) 1–12. https://doi.org/10.1142/S2339547817300013.

[4] J.-S. Chen, T.-Y. Liu, H.-M. Tsou, Y.-S. Ting, Y.-Q. Tseng, C.-H. Wang, Biopolymer brushes grown on PDMS contact lenses by in situ atmospheric plasma-induced polymerization, J Polym Res. 24 (2017) 69. https://doi.org/10.1007/s10965-017-1230-7.

[5] C.S.A. Musgrave, F. Fang, Contact Lens Materials: A Materials Science Perspective, Materials. 12 (2019) 261. https://doi.org/10.3390/ma12020261.

[6] K.W. Dunn, P.N. Hall, C.T.K. Khoo, Breast implant materials: sense and safety, British Journal of Plastic Surgery. 45 (1992) 315–321. https://doi.org/10.1016/0007-1226(92)90060-B.

[7] A. Daniels, Silicone breast implant materials, Swiss Med Wkly. (2012). https://doi.org/10.4414/smw.2012.13614.

[8] V. Bartzoka, M.R. McDermott, M.A. Brook, Protein-Silicone Interactions, Adv. mater. (1999), 11, 3. https://doi.org/10.1021/la9711140

[9] M. Mempin, H. Hu, D. Chowdhury, A. Deva, K. Vickery, The A, B and C's of Silicone Breast Implants: Anaplastic Large Cell Lymphoma, Biofilm and Capsular Contracture, Materials. 11 (2018) 2393. https://doi.org/10.3390/ma11122393.

[10] S.L. Spear, J.L. Baker, Classification of Capsular Contracture after Prosthetic Breast Reconstruction, Plastic and Reconstructive Surgery. (1995) 1119–1123. https://doi.org/10.1097/00006534-199510000-00018.

[11] S. Fischer, C. Hirche, M.A. Reichenberger, J. Kiefer, Y. Diehm, S. Mukundan, M. Alhefzi, E.M. Bueno, U. Kneser, B. Pomahac, Silicone Implants with Smooth Surfaces Induce Thinner but Denser Fibrotic Capsules Compared to Those with Textured Surfaces in a Rodent Model, PLoS ONE. 10 (2015) e0132131. https://doi.org/10.1371/journal.pone.0132131.

[12] A. Marra, G. Viale, S.A. Pileri, G. Pravettoni, G. Viale, F. De Lorenzi, F. Nolè, P. Veronesi, G. Curigliano, Breast implant-associated anaplastic large cell lymphoma: A comprehensive review, Cancer Treatment Reviews. 84 (2020) 101963. https://doi.org/10.1016/j.ctrv.2020.101963.

[13] N. Mehta-Shah, M.W. Clemens, S.M. Horwitz, How I treat breast implant–associated anaplastic large cell lymphoma, Blood. 132 (2018) 1889–1898. https://doi.org/10.1182/blood-2018-03-785972.

[14] A. Chacko, T. Lloyd, Breast implant-associated anaplastic large cell lymphoma: a pictorial review, Insights Imaging. 9 (2018) 683–686. https://doi.org/10.1007/s13244-018-0652-z.

[15] J.J. Keech, B.J. Creech, Anaplastic T-cell lymphoma in proximity to a saline-filled breast implant, (1997). https://doi.org/10.1097/00006534-199708000-00065.

[16] https://www.fda.gov/medical-devices/implants-and-prosthetics/breast-implants, (2020).

[17] M. Lee, G. Ponraja, K. McLeod, S. Chong, Breast Implant Illness: A Biofilm Hypothesis, Plastic and Reconstructive Surgery - Global Open. 8 (2020) e2755. https://doi.org/10.1097/GOX.0000000000002755.

[18] P. S V V S Narayana, P. S V V Srihari, Biofilm Resistant Surfaces and Coatings on Implants: A Review, Materials Today: Proceedings. 18 (2019) 4847–4853. https://doi.org/10.1016/j.matpr.2019.07.475.

[19] U.M. Rieger, J. Mesina, D.F. Kalbermatten, M. Haug, H.P. Frey, R. Pico, R. Frei, G. Pierer, N.J. Lüscher, A. Trampuz, Bacterial biofilms and capsular contracture in patients with breast implants: Breast capsular contracture and bacterial biofilm, Br J Surg. 100 (2013) 768–774. https://doi.org/10.1002/bjs.9084.

[20] H. Hu, K. Johani, A. Almatroudi, K. Vickery, B. Van Natta, M.E. Kadin, G. Brody, M. Clemens, C.Y. Cheah, S. Lade, P.A. Joshi, H.M. Prince, A.K. Deva, Bacterial Biofilm Infection Detected in Breast Implant–Associated Anaplastic Large-Cell Lymphoma:, Plastic and Reconstructive Surgery. 137 (2016) 1659–1669. https://doi.org/10.1097/PRS.0000000000002010.

[21] M. Lam, V. Migonney, C. Falentin-Daudre, Review of silicone surface modification techniques and coatings for antibacterial/antimicrobial applications to improve breast implant surfaces, Acta Biomaterialia. 121 (2021) 68–88. https://doi.org/10.1016/j.actbio.2020.11.020.

[22] M. Lam, V. Moris, V. Humblot, V. Migonney, C. Falentin-Daudre, A simple way to graft a bioactive polymer – Polystyrene sodium sulfonate on silicone surfaces, European Polymer Journal. 128 (2020) 109608. https://doi.org/10.1016/j.eurpolymj.2020.109608.

[23] A.-C. Crémieux, G. Pavon-Djavid, A.S. Mghir, G. Hélary, V. Migonney, Bioactive Polymers Grafted on Silicone to Prevent Staphylococcus Aureus Prosthesis Adherence: In Vitro and in VIVO Studies, (n.d.) 8.

[24] H.P. Felgueiras, I.B. Aissa, M.D.M. Evans, V. Migonney, Contributions of adhesive proteins to the cellular and bacterial response to surfaces treated with bioactive polymers: case of poly(sodium styrene sulfonate) grafted titanium surfaces, Journal of Materials

Science: Materials in Medicine. 26 (2015) 261–275. https://doi.org/10.1007/s10856-015-5596-y.

[25] H. Chouirfa, M.D.M. Evans, P. Bean, A. Saleh-Mghir, A.C. Crémieux, D.G. Castner, C. Falentin-Daudré, V. Migonney, Grafting of Bioactive Polymers with Various Architectures: A Versatile Tool for Preparing Antibacterial Infection and Biocompatible Surfaces, ACS Appl. Mater. Interfaces. 10 (2018) 1480–1491. https://doi.org/10.1021/acsami.7b14283.

[26] Q. Xu, M. Pang, L. Zhu, Y. Zhang, S. Feng, Mechanical properties of silicone rubber composed of diverse vinyl content silicone gums blending, Materials & Design. 31 (2010) 4083–4087. https://doi.org/10.1016/j.matdes.2010.04.052.

[27] J. Wu, K. Niu, B. Su, Y. Wang, properties of silicone elastomer, Polymer Degradation and Stability. (2018) 10.

[28] S. Necchi, D. Molina, S. Turri, F. Rossetto, M. Rietjens, G. Pennati, Failure of silicone gel breast implants: Is the mechanical weakening due to shell swelling a significant cause of prostheses rupture?, Journal of the Mechanical Behavior of Biomedical Materials. 4 (2011) 2002–2008. https://doi.org/10.1016/j.jmbbm.2011.06.019.

[29] D. Oldfield, T. Symes, Long term natural ageing of silicone elastomers, Polymer Testing. 15 (1996) 115–128. https://doi.org/10.1016/0142-9418(95)00018-6.

[30] ISO (the International Organization for Standardization), https://www.iso.org/obp/ui/fr/#iso:std:iso:14607:ed-3:v2:en (accessed February 11, 2021).

[31] J.N. Lee, C. Park, G.M. Whitesides, Solvent Compatibility of Poly(dimethylsiloxane)-Based Microfluidic Devices, Anal. Chem. 75 (2003) 6544–6554. https://doi.org/10.1021/ac0346712.

[32] P.J. Flory, J. Rehner, Statistical Mechanics of Cross-Linked Polymer Networks II. Swelling, The Journal of Chemical Physics. 11 (1943) 521–526. https://doi.org/10.1063/1.1723792.

[33] Z. Tan, R. Jaeger, G.J. Vancso, Crosslinking studies of poly(dimethylsiloxane) networks: a comparison of inverse gas chromatography, swelling experiments and mechanical analysis, Polymer. 35 (1994) 3230–3236. https://doi.org/10.1016/0032-3861(94)90127-9.

[34] A.A. Valencia-Lazcano, T. Alonso-Rasgado, A. Bayat, Characterisation of breast implant surfaces and correlation with fibroblast adhesion, Journal of the Mechanical Behavior of Biomedical Materials. 21 (2013) 133–148. https://doi.org/10.1016/j.jmbbm.2013.02.005.

[35] A. Loch-Wilkinson, K.J. Beath, R.J.W. Knight, W.L.F. Wessels, M. Magnusson, T. Papadopoulos, T. Connell, J. Lofts, M. Locke, I. Hopper, R. Cooter, K. Vickery, P.A. Joshi, H.M. Prince, A.K. Deva, Breast Implant–Associated Anaplastic Large Cell Lymphoma in Australia and New Zealand: High-Surface-Area Textured Implants Are Associated with Increased Risk, Plastic and Reconstructive Surgery. 140 (2017) 645–654. https://doi.org/10.1097/PRS.0000000000003654.

[36] P. Jones, M. Mempin, H. Hu, D. Chowdhury, M. Foley, R. Cooter, W.P. Adams, K. Vickery, A.K. Deva, The Functional Influence of Breast Implant Outer Shell Morphology on Bacterial Attachment and Growth:, Plastic and Reconstructive Surgery. 142 (2018) 837–849. https://doi.org/10.1097/PRS.0000000000004801.

[37] International Organization for Standardization, “UNI EN ISO 10993-5: 2009,” in Biological evaluation of medical devices–part 5: in vitro cytotoxicity testing, International Organization for Standardization, Geneva, Switzerland, 2009., (n.d.).

[38] M. Li, K.G. Neoh, L.Q. Xu, R. Wang, E.-T. Kang, T. Lau, D.P. Olszyna, E. Chiong, Surface Modification of Silicone for Biomedical Applications Requiring Long-Term

Antibacterial, Antifouling, and Hemocompatible Properties, Langmuir. 28 (2012) 16408–16422. https://doi.org/10.1021/la303438t.

[39] M. Ravikanth, K. Manjunath, C. Ramachandran, P. Soujanya, T. Saraswathi, Heterogenecity of fibroblasts, J Oral Maxillofac Pathol. 15 (2011) 247. https://doi.org/10.4103/0973-029X.84516.